

Experimental demonstration of rotational varifocal moiré metalens

Kentaro Iwami,* Chikara Ogawa, Tomoyasu Nagase, and Satoshi Ikezawa

*Department of Mechanical Systems Engineering,
Tokyo University of Agriculture and Technology, Koganei, Tokyo 184-8588 Japan*

E-mail: k_iwami@cc.tuat.ac.jp

Phone: +81 (0)42 3887658. Fax: +81 (0)42 3887657

Abstract

This paper reports experimental demonstration of moiré metalens with a wide focal length tunability from negative to positive through mutual angle rotation at a wavelength of 900 nm. The moiré metalens was developed using high-index contrast transmit array meta-atoms composed of amorphous silicon octagonal pillars designed to have polarization insensitivity and full 2π phase coverage. The designed moiré metalens was fabricated on a glass substrate using simple a-Si sputter deposition, electron beam lithography through character projection, metal mask lift-off, and reactive-ion silicon etching. The moiré metalens has focal length tunability ranges from $-\infty$ to -1.73 mm, and from 1.73 mm to ∞ , corresponding to an optical power in the range $-578 - 578 \text{ m}^{-1}$ at a mutual rotation between $\pm 90^\circ$. Our results reveal a proof of concept for focal length tuning with mutual rotation of lens components based on moiré lens configuration at optical frequencies.

Keywords

dielectric metasurfaces, varifocal metalens, moiré lens, amorphous silicon, waveguides

Introduction

Metasurfaces, a planar branch of metamaterials, have attracted significant attention because they can tailor optical wavefront by arranging subwavelength patterns (meta-atoms) on surfaces.¹⁻³ They can demonstrate unique optical properties that cannot be achieved with natural materials and have high affinity for micro/nanofabrication methods, including lithography, deposition, and etching. Therefore, metasurfaces have opened many research fields and have several applications, including lenses,⁴⁻⁶ retarders and waveplates,⁷⁻¹⁰ vector beam converters,¹¹⁻¹³ color filters,¹⁴⁻¹⁶ and holography.¹⁷⁻²⁰ It should be emphasized that mechanical deformation or change of mutual geometric position of metasurfaces offer novel functionalities and tunability for their optical properties. Reconfigurable metasurfaces have been studied based on this idea, including tunable transmittance,²¹ color tuning,²² and active phase shifters.^{23,24}

Metasurface lenses, or metalens, has attracted considerable attention owing to their thinness and lightweight. The recent development of lossless dielectric metalens^{5,6,25} have also stimulated the attention in this field. Tunable focal length, or varifocal lens, are a promising and expected functionality of metalens. Similar to conventional refractive lens doublet, the longitudinal motion of lens along with the optical axis have been demonstrated based on micro-electromechanical actuators.²⁶ However, the effect of the pull-in instability of the electrostatic parallel plates actuator limits the travel range of metalens,^{27,28} resulting in a narrow tunable range for the focal length.

Since metalens has a high degree of design freedom, it is not necessary to make the tuning method for the focal length similar to conventional refractive lenses. It is desirable to study how diffractive optical element (DOE) techniques or diffractive lenses can be applied

to metalens. In fact, a DOE-inspired tunable metalens, the Alvarez metalens, has been experimentally demonstrated with focal length tuning based on the lateral movement of a pair of lenses.²⁹⁻³¹ However, the lateral motion of Alvarez lenses limits the effective area of the lenses. Furthermore, the reported focal length range of mechanically tunable metalens is limited to the positive region.

Moiré lenses are a pair of axially asymmetric lenses that achieve tunable focal length with mutual rotation, as presented in Fig. 1(a).^{32,33} They offer a wide range of focal lengths from negative to positive and has been realized using DOE.³⁴ Moiré metalens has also been studied using numerical simulations,^{35,36} and has been demonstrated in the microwave frequency band quite recently.³⁷ However, the demonstration at optical frequencies has not been reported yet due to the difficulty of fabricating at such frequencies.

In this paper, we experimentally demonstrate tunable focal length using moiré metalens at the near infrared frequency band using polarization-insensitive meta-atoms based on high-index contrast transmit arrays (HCTAs), which are made of amorphous silicon (a-Si) in this case. We designed a-Si octagonal pillars with polarization insensitivity and full 2π phase coverage at a wavelength of 900 nm. The metalens were designed to satisfy the phase distribution of moiré metalens, as detailed below, by hexagonally mapping the corresponding pillars to each lattice points. The metalens was fabricated on a silicon substrate using simple a-Si sputter deposition, electron beam lithography through character projection, metal mask lift-off, and reactive-ion etching (RIE) of silicon. The fabricated metalens exhibited focal length tunability at the ranges from $-\infty$ to -1.73 mm and from $+1.73$ mm to $+\infty$ at a mutual rotation of $\pm 90^\circ$ at 900 nm. The results reported here reveal a proof of concept for focal length tuning with mutual rotation of lens components based on moiré lens configuration at optical frequencies, and thus paving way for applications in optical frequencies, including near infrared, visible, and ultraviolet wavelengths.

Design and Fabrication of Moiré Metalens

Figure 1 presents a schematic diagram of moiré metalens. It consists of two metalenses, as shown in Fig. 1(a), and their total focal length can be tuned by mutual rotation from negative to positive. Each of the moiré metalens pair is designed with transmission function distributions in polar coordinates (r, φ) :³²

$$\begin{aligned} T_1(r, \varphi) &= \exp \{i\text{round}(ar^2)\varphi\} \\ T_2(r, \varphi) &= \exp \{-i\text{round}(ar^2)\varphi\} \end{aligned} \quad (1)$$

where a is a constant. The phase distribution of the first lens T_1 is presented in Fig. 1(b). With mutual rotation angle of θ , the joint transmission function can be expressed as:

$$T_{\text{joint}} = T_1(r, \varphi)T_2(r, \varphi - \theta) = \exp \{i\text{round}(ar^2)\theta\}. \quad (2)$$

This equation is similar to that for spherical lenses under paraxial approximation, $T = \exp(i\pi r^2/f\lambda)$, where f and λ represent the focal length and the wavelength, respectively. Therefore, by adjusting the constant a to satisfy equation $f^{-1} = a\theta\lambda/\pi$, the optical power f^{-1} becomes proportional to θ . Note that the round function is used to avoid the sectoring effect.³²

Figures 1(c-e) presents the phase distributions of the second metalens with mutual rotation angles of $+30^\circ$, $+60^\circ$, and -60° , respectively, together with the total phase distributions superimposed with the first metalens (Fig. 1(b)). Positive rotation angles create total phase distribution similar to convex Fresnel lenses, whereas and larger rotation angles give rise to higher phase gradient, which corresponds to short focal length and higher optical power, as presented in Figs. 1(c) and (d). In contrast, as presented in Fig. 1(e), a negative rotation angle creates concave-like phase distribution. We show that adopting moiré metalens leads to focal lengths with a wide tuning range from negative to positive.

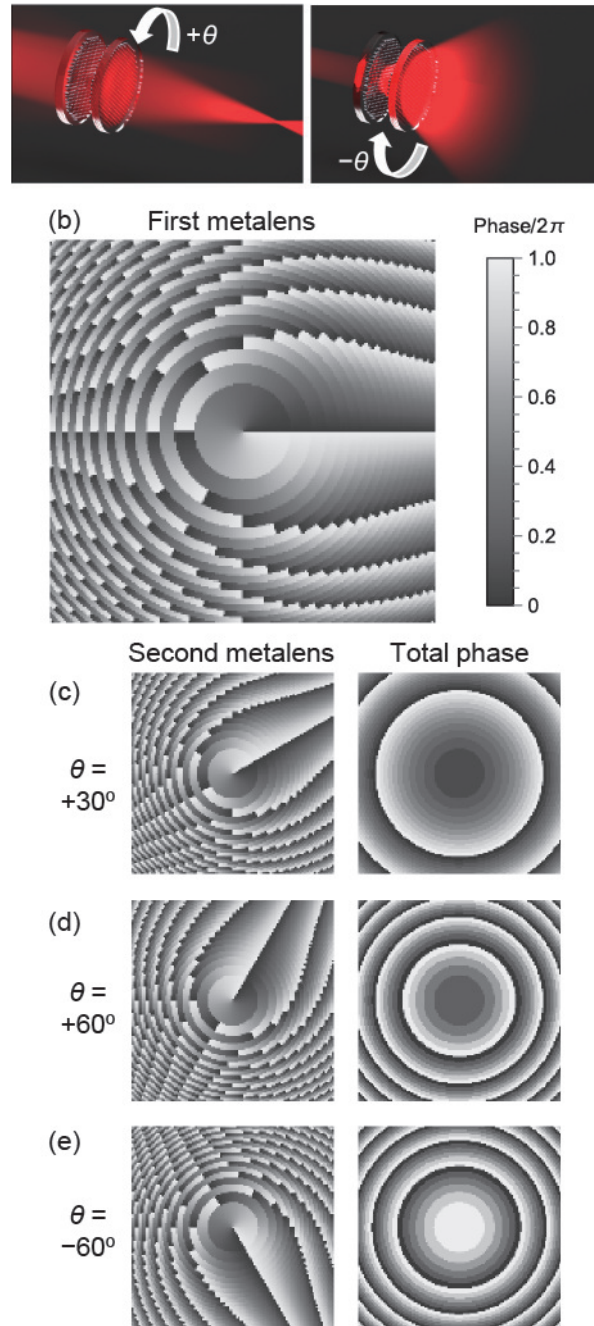


Figure 1: Principle of moiré metalens. (a) Schematic drawing of working principle. (b) Phase distribution of one of two lenses. (c–e) Phase distributions of second lens and combined moiré metalens for various mutual rotation angles θ for focal length, f tuning. Note that the same color legends are used throughout (b–e).

We adopted a-Si octagonal pillar HCTAs as polarization-insensitive meta-atoms.²⁵ Electromagnetic simulation was conducted using the commercially available finite element software, COMSOL Multiphysics ver. 5.1 (COMSOL Inc., USA), as presented in Fig. 2. A schematic diagram of the simulation setup is presented in Figure 2(a). An octagonal pillar with a period of 400 nm was situated on the silica glass substrate, with air as the surrounding medium (not shown). X -polarized light at a wavelength of 900 nm was incident from the glass bottom side, whereas the transmittance and phase delay of the pillar was evaluated at the output port (air side). The perfect electric conductor (PEC) boundary condition was applied to the $\pm x$ boundaries, whereas the Floquet periodic condition was applied to other boundaries. An a-Si material parameter was used as an Si pillar.³⁸

Figure 2(b) presents the results of parameter sweep for transmittance and phase/ 2π , which is obtained by changing the pillar width and height in 10-nm steps. We found that the region around height > 380 nm achieves both high transmittance and full 2π phase coverage. Figure 2(c) presents the x -component of electric field, E_x distribution at a pillar height of 400 nm, and widths of 90, 240, and 300 nm, respectively. It is clearly shown that the phase difference between the 240, 300, and 90 nm pillars at the output port (top of the image) correspond to π and 2π , respectively. Therefore, considering fabrication process limitations for high-aspect-ratio structures, we adopted pillars with 400-nm height as a meta atoms.

We used these octagonal pillars as meta-atoms to design moiré metalens with a diameter of 2 mm with maximum optical powers of $f^{-1} = \pm(1.73 \text{ mm})^{-1}$ at a mutual rotation angle of $\theta = \pm 90^\circ$. This corresponds to a maximum numerical aperture (NA) of 0.5 for the moiré metalens. We prepared a GDSII CAD file of the moiré metalens by mapping pillars with corresponding phase delays satisfying the phase distribution described by T_1 of equation 1 to each hexagonal lattice point with the pitch of 400 nm using a Python library Gdspy.

We fabricated a metalens on a quartz glass substrate, sputter-depositing an amorphous silicon film with a thickness of 400 nm. A lens pattern with a diameter of 2 mm was drawn by

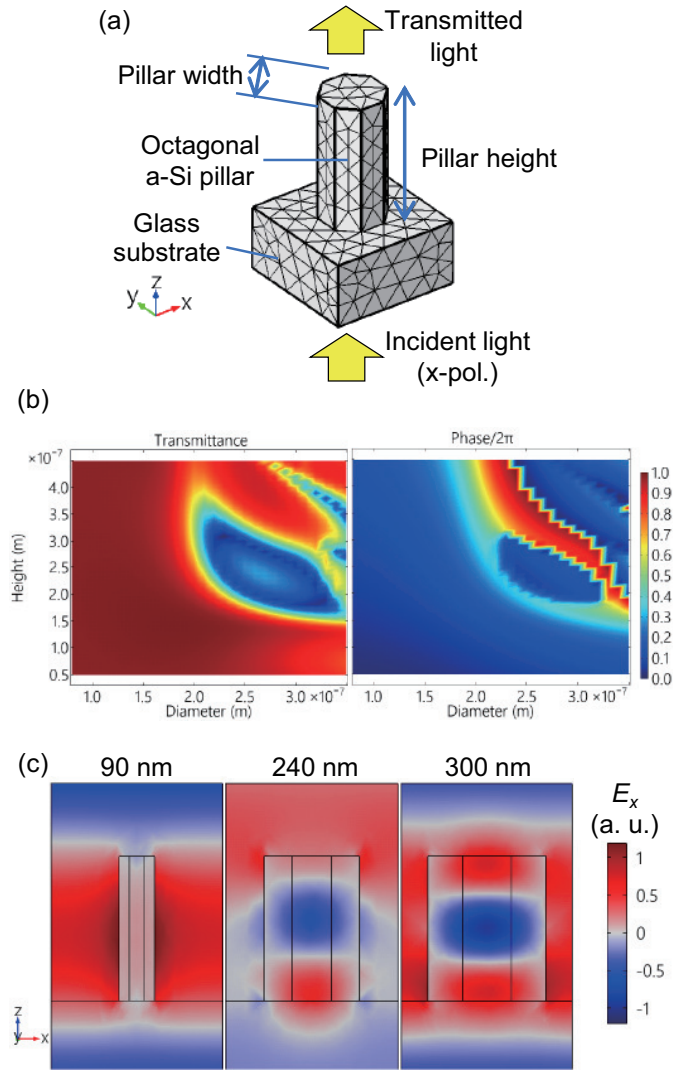


Figure 2: COMSOL simulation of a-Si octagonal pillar meta-atom. (a) Calculation model. (b) Parameter mapping of transmittance and phase/ 2π , sweeping pillar height, and width. (c) Electric field (E_x) distribution of a-Si octagonal pillars with widths of 90, 240, and 300 nm, respectively.

electron beam lithography using character projection (CP) (Advantest F7000-S, Advantest, Japan), employing dedicated octagonal stencil masks to achieve high-throughput drawing. The GDSII CAD file described above was converted into a CP shot data with proximity effect compensation. After the resist development, an aluminum mask was patterned on the a-Si film through lift-off process. Si pillars were formed by RIE. Finally, the aluminum mask was removed using a solution of phosphoric, nitric, and acetic acids mixture.

Results and Discussion

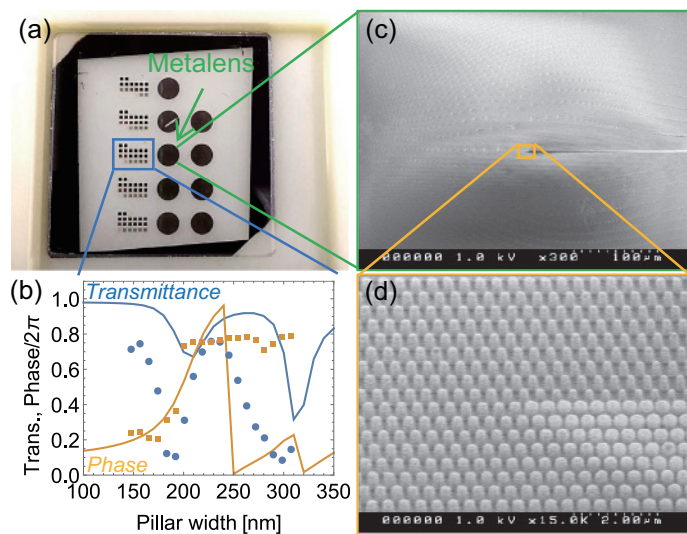


Figure 3: Fabricated metalens. (a) Photograph of the fabricated lenses on a 2-cm-square glass substrate. The nine circles represent 2-mm-diameter metalenses. Blue-indicated square patterns are pillar arrays with constant widths for transmission property measurements. (b) Transmission properties at a wavelength of 900 nm. The dots indicate measurement results, whereas the lines indicate COMSOL simulation. Blue and orange correspond to transmittance and phase/ 2π , respectively. (c) SEM images of the lens and (d) its close-up to the center, observed with 45° tilting angles.

Figure 3 represents (a) a photograph of the fabricated lenses on a 2-cm-square glass substrate, (b) transmission properties, and scanning electron microscope (SEM) images (c–d). In Fig. 3(a), the nine circles are 2-mm-diameter metalenses. Blue-indicated square patterns are pillar arrays with constant widths for transmission property measurements.

Figure 3(b) presents the transmission properties of the pillars as a function of pillar width at a wavelength of 900 nm. The dots indicate the measurement results, and the lines represent COMSOL simulation results. Blue and orange correspond to transmittance and phase/ 2π , respectively. The data points in Fig. 3(b) are based on the measured widths of pillars. The phase delays of the pillars were measured by the interference method,³⁹ using a laser diode and a microspectroscopic system (Techno Synergy, DF-1037). Figure 3(c) presents the SEM image of the lens, and 3(d) shows its close-up to the center, which is observed at 45° angles. We fabricated width-distributed pillars. However, the pillars are cylindrical instead of octagonal due to fabrication limitations.

The phase delay rapidly increases for both the simulation and experiment as the width increases, as presented in Fig. 3(b). Though the experimental transmittance is lower than that of the simulation, the position of the dips is similar. The disparity between the experiment and simulation can be attributed to fabrication error, including the rounded shape of the pillar top presented in 3(d).

Figure 4 presents the experimental setup for focal length measurement. The optical system is presented in Fig. 4(a). It uses tungsten halogen white light as a source. The incident light passes through a band pass filter (#65-184, Edmund Optics USA, OD = 4, center wavelength = 904 nm, FWHM = 10 nm) and a test target (USAF 1951). We prepared the moiré metalens sample by assembling two metalens pieces fabricated using the above-mentioned process. The latter lens was flipped upside down along the horizontal axis to satisfy the phase distribution of T_2 in equation 1. These lenses are aligned carefully under the microscope observation, and adhered using a tape with certain mutual rotation angles θ . The transmitted image of a USAF target captured using a CMOS camera (DCC1545M, Thorlab Co., USA) with a $20\times$ objective lens and iris.

Figure 4(b) presents images captured without the moiré metalens and focused onto the test target. A bright part due to the light source can be seen at the center. Figure 4(c) presents the image focused on the moiré metalens doublet. The lens diameter of 2 mm was

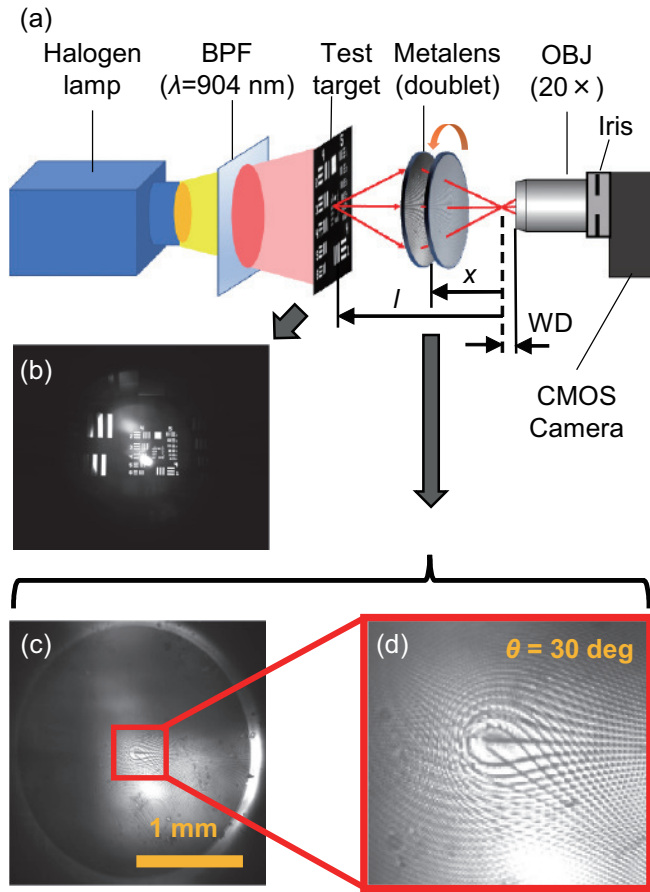


Figure 4: Experimental setup for focal length measurement. (a) Optical system. (b) Image focused on the target without moiré metalens, showing the iris circle. (c) Image focused on the moiré metalens and (d) its magnified version. Mutual rotation angle can be determined from the image.

almost equivalent to the opening of the iris. Figure 4(d) presents the magnified image of (c). The mutual rotation angle of $\theta = 30$ deg. are clearly seen.

Using the metalens position x from the image plane and target position l as shown in 4(a) under the certain mutual rotation angle θ , the focal length $f(\theta)$ of the moiré metalens was calculated using the following equation,

$$\frac{1}{f(\theta)} = \frac{1}{l-x} + \frac{1}{x}. \quad (3)$$

Figure 5 presents (a) the measurement results for focal length and (b–e) typical imaging results. In Fig. 5(a), the circle markers indicate the experimental results obtained from the setup presented in Fig. 4. The dashed curve indicates the designed characteristics, $f = \pi/(a\lambda\theta)$. Note that the standard deviation of the data points is lower than the diameter of each marker. The experimental results are consistent with the design, and we demonstrated focal length tuning from negative to positive; (b) and (c) present captured images at nominal rotation angles of -60° and $+60^\circ$, respectively; (d) and (e) present magnified images of (b) and (c). Inversed real images are presented in (c) and (e), which correspond to the positive focal length. In contrast, straight virtual images are presented in (b) and (d), corresponding to the negative focal length.

Our results reveal a wide range of tunability, and this is the first report on the focal length tuning from negative to positive. In fact, metalens can be tuned both as a convex and concave lens. Though we adopted alignment and adhesion processes in this paper, MEMS-actuated rotational stages have been reported, whereas microrotational varifocal metalens can be realized by proper integration with actuators. In this work, we employed a 2-mm-diameter lens, which can be extended to a cm-scale in principle due to the high throughput of CP-based EB lithography.

In conclusion, we experimentally demonstrated a rotational varifocal metalens or moiré metalens. The metalens was designed using polarization-insensitive a-Si HCTAs as meta-

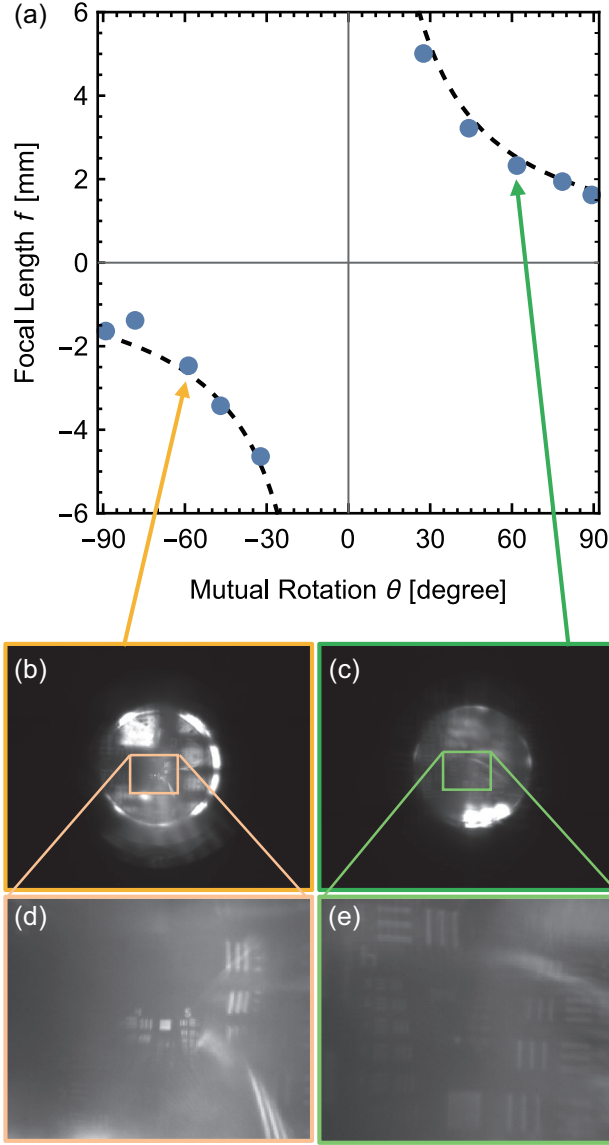


Figure 5: (a) Measurement results for focal length and (b–e) typical imaging results . In (a), the circle markers indicate the experimental results obtained from the setup presented in Fig. 4. The dashed curve indicates the designed characteristics $f = \pi/(a\lambda\theta)$. (b) and (c) present captured images at the nominal rotation angles of -60° and $+60^\circ$, respectively, and (d) and (e) present their magnified images. Inverted real images are presented in (c) and (e), whereas straight virtual images are presented in (b) and (d).

atoms. We investigated the fabricated metalens at a wavelength of 900 nm and demonstrated focal length tuning at the ranges from $-\infty$ to -1.73 mm and from $+1.73$ mm to $+\infty$ at a mutual rotation between $\pm 90^\circ$, which corresponds to an optical power tuning between ± 578 m⁻¹.

Author Information

Corresponding Author

E-mail: k_iwami@cc.tuat.ac.jp (K. Iwami)

ORCID

Kentaro Iwami: 0000-0002-4458-5704

Satoshi Ikezawa: 0000-0001-6184-7123

Author Contributions

K. I. conceived the idea of moiré metalens, performed COMSOL simulation, and supervised the project. K. I. and C. O. designed and fabricated the moiré metalens. K. I. and T. N. performed measurements of phase delay of Si pillars. C. O. and S. I. performed measurements of focal length. K. I. wrote the initial draft of the manuscript. All authors analyzed and discussed the results and contributed to writing the manuscript. All authors have given approval to the final version of the manuscript.

Notes

The authors declare no competing financial interest.

Acknowledgement

This research was supported by Japanese Society for the Promotion of Science (JSPS) Grant-in-Aid for Scientific Research (KAKENHI) B Grant Number JP17H02754, Nanotechnology Platform site at the University of Tokyo, which is supported by the Ministry of Education, Culture, Sports, Science and Technology (MEXT), Japan. The authors thank Prof. Yoshio Mita, and Dr. Eric Lebrasseur for their help about electron beam lithography and reactive ion etching, and Prof. Kuniaki Konishi for his help about ellipsometry. The numerical calculations were carried out on the TSUBAME3.0 supercomputer at Tokyo Institute of Technology.

References

- (1) Zheludev, N. I.; Kivshar, Y. S. From metamaterials to metadevices. *Nature Materials* **2012**, *11*, 917–924.
- (2) Glybovski, S. B.; Tretyakov, S. A.; Belov, P. A.; Kivshar, Y. S.; Simovski, C. R. Metasurfaces: From microwaves to visible. *Physics Reports* **2016**, *634*, 1–72.
- (3) Yu, N.; Capasso, F. Flat optics with designer metasurfaces. *Nature Materials* **2014**, *13*, 139–150.
- (4) Ni, X.; Ishii, S.; Kildishev, A. V.; Shalaev, V. M. Ultra-thin, planar, Babinet-inverted plasmonic metalenses. *Light: Science & Applications* **2013**, *2*, e72.
- (5) Khorasaninejad, M.; Chen, W. T.; Devlin, R. C.; Oh, J.; Zhu, A. Y.; Capasso, F. Metalenses at visible wavelengths: Diffraction-limited focusing and subwavelength resolution imaging. *Science* **2016**, *352*, 1190–1194.
- (6) Wang, S. et al. A broadband achromatic metalens in the visible. *Nature Nanotechnology* **2018**, *13*, 227–232.

- (7) Kats, M. A.; Genevet, P.; Aoust, G.; Yu, N.; Blanchard, R.; Aieta, F.; Gaburro, Z.; Capasso, F. Giant birefringence in optical antenna arrays with widely tailorable optical anisotropy. *Proceedings of the National Academy of Sciences of the United States of America* **2012**, *109*, 12364–12368.
- (8) Yu, N.; Aieta, F.; Genevet, P.; Kats, M. A.; Gaburro, Z.; Capasso, F. A Broadband, Background-Free Quarter-Wave Plate Based on Plasmonic Metasurfaces. *Nano Letters* **2012**, *12*, 6328–6333.
- (9) Ishii, M.; Iwami, K.; Umeda, N. An Au nanofin array for high efficiency plasmonic optical retarders at visible wavelengths. *Applied Physics Letters* **2015**, *106*, 021115.
- (10) Ishii, M.; Iwami, K.; Umeda, N. Highly-efficient and angle-independent zero-order half waveplate at broad visible wavelength based on Au nanofin array embedded in dielectric. *Optics Express* **2016**, *24*, 7966–7976.
- (11) Genevet, P.; Yu, N.; Aieta, F.; Lin, J.; Kats, M. A.; Blanchard, R.; Scully, M. O.; Gaburro, Z.; Capasso, F. Ultra-thin plasmonic optical vortex plate based on phase discontinuities. *Applied Physics Letters* **2012**, *100*, 013101.
- (12) Iwami, K.; Ishii, M.; Kuramochi, Y.; Ida, K.; Umeda, N. Ultrasmall radial polarizer array based on patterned plasmonic nanoslits. *Applied Physics Letters* **2012**, *101*, 161119.
- (13) Hakobyan, D.; Magallanes, H.; Seniutinas, G.; Juodkazis, S.; Brasselet, E. Tailoring Orbital Angular Momentum of Light in the Visible Domain with Metallic Metasurfaces. *Advanced Optical Materials* **2016**, *4*, 306–312.
- (14) Ikeda, N.; Sugimoto, Y.; Ochiai, M.; Tsuya, D.; Koide, Y.; Inoue, D.; Miura, A.; Nomura, T.; FUJIKAWA, H.; Sato, K. Color Filter Based on Surface Plasmon Resonance Utilizing Sub-Micron Periodic Hole Array in Aluminum Thin Film. *IEICE Transactions on Electronics* **2012**, *E95-C*, 251–254.

- (15) Nagasaki, Y.; Suzuki, M.; Hotta, I.; Takahara, J. Control of Si-Based All-Dielectric Printing Color through Oxidation. *ACS Photonics* **2018**, *5*, 1460–1466.
- (16) Nagasaki, Y.; Hotta, I.; Suzuki, M.; Takahara, J. Metal-Masked Mie-Resonant Full-Color Printing for Achieving Free-Space Resolution Limit. *ACS Photonics* **2018**, *5*, 3849–3855.
- (17) Huang, L.; Chen, X.; Mühlenbernd, H.; Zhang, H.; Chen, S.; Bai, B.; Tan, Q.; Jin, G.; Cheah, K.-W.; Qiu, C.-W.; Li, J.; Zentgraf, T.; Zhang, S. Three-dimensional optical holography using a plasmonic metasurface. *Nature communications* **2013**, *4*, 2808.
- (18) Yifat, Y.; Eitan, M.; Iluz, Z.; Hanein, Y.; Boag, A.; Scheuer, J. Highly Efficient and Broadband Wide-Angle Holography Using Patch-Dipole Nanoantenna Reflectarrays. *Nano Letters* **2014**, *14*, 2485–2490.
- (19) Huang, Y.-W.; Chen, W. T.; Tsai, W.-Y.; Wu, P. C.; Wang, C.-M.; Sun, G.; Tsai, D. P. Aluminum Plasmonic Multicolor Meta-Hologram. *Nano Letters* **2015**, *15*, 3122–3127.
- (20) Wan, W.; Gao, J.; Yang, X. Full-Color Plasmonic Metasurface Holograms. *ACS Nano* **2016**, *10*, 10671–10680.
- (21) Ou, J. Y.; Plum, E.; Jiang, L.; Zheludev, N. I. Reconfigurable Photonic Metamaterials. *Nano Letters* **2011**, *11*, 2142–2144.
- (22) Honma, H.; Takahashi, K.; Ishida, M.; Sawada, K. A Low-Voltage and High Uniformity Nano-Electro-Mechanical System Tunable Color Filter Based on Subwavelength Grating. *Japanese Journal of Applied Physics* **2012**, *51*, 11PA01.
- (23) Yamaguchi, K.; Yamanaka, H.; Ohtsu, T.; Ishii, S. Electrically driven plasmon chip: Active plasmon lens in the visible range. *Applied Physics Letters* **2016**, *108*, 111903.
- (24) Shimura, T.; Kinoshita, T.; Koto, Y.; Umeda, N.; Iwami, K. Birefringent reconfigurable

- metasurface at visible wavelengths by MEMS nanograting. *Applied Physics Letters* **2018**, *113*, 171905.
- (25) Arbabi, A.; Horie, Y.; Ball, A. J.; Bagheri, M.; Faraon, A. Subwavelength-thick lenses with high numerical apertures and large efficiency based on high-contrast transmitarrays. *Nature Communications* **2015**, *6*, 1–6.
- (26) Arbabi, E.; Arbabi, A.; Kamali, S. M.; Horie, Y.; Faraji-Dana, M.; Faraon, A. MEMS-tunable dielectric metasurface lens. *Nature Communications* **2018**, *9*, 812.
- (27) Hung, E. S.; Senturia, S. D. Extending the travel range of analog-tuned electrostatic actuators. *Journal of Microelectromechanical Systems* **1999**, *8*, 497–505.
- (28) Nemirovsky, Y.; Zelniker, I.; Degani, O.; Sarusi, G. A methodology and model for the pull-in parameters of magnetostatic actuators. *Journal of Microelectromechanical Systems* **2005**, *14*, 1253–1264.
- (29) Zhang, P.; Zhang, X.; Xu, S.; Lu, P.; Tan, D.; Xu, J.; Wang, F.; Jiang, L.; Chen, K. Phosphorus doping effect on linear and nonlinear optical properties of Si/SiO₂ multilayers. *Optical Materials Express* **2017**, *7*, 304.
- (30) Colburn, S.; Zhan, A.; Majumdar, A. Varifocal zoom imaging with large area focal length adjustable metalenses. *Optica* **2018**, *5*, 825.
- (31) Colburn, S.; Majumdar, A. Simultaneous Achromatic and Varifocal Imaging with Quartic Metasurfaces in the Visible. *ACS Photonics* **2019**, acsphotronics.9b01216.
- (32) Bernet, S.; Ritsch-Martel, M. Adjustable refractive power from diffractive moiré elements. *Applied Optics* **2008**, *47*, 3722.
- (33) Bernet, S.; Ritsch-Martel, M. Multi-color operation of tunable diffractive lenses. *Optics Express* **2017**, *25*, 2469.

- (34) Bernet, S.; Harm, W.; Ritsch-Marte, M. Demonstration of focus-tunable diffractive Moiré-lenses. *Optics Express* **2013**, *21*, 6955.
- (35) Yilmaz, N.; Ozdemir, A.; Ozer, A.; Kurt, H. Rotationally tunable polarization-insensitive single and multifocal metasurface. *Journal of Optics* **2019**, *21*, 045105.
- (36) Liu, Z.; Du, Z.; Hu, B.; Liu, W.; Liu, J.; Wang, Y. Wide-angle Moiré metalens with continuous zooming. *Journal of the Optical Society of America B* **2019**, *36*, 2810.
- (37) Guo, Y.; Pu, M.; Ma, X.; Li, X.; Shi, R.; Luo, X. Experimental demonstration of a continuous varifocal metalens with large zoom range and high imaging resolution. *Applied Physics Letters* **2019**, *115*, 1–6.
- (38) Pierce, D. T.; Spicer, W. E. Electronic structure of amorphous Si from photoemission and optical studies. *Physical Review B* **1972**, *5*, 3017–3029.
- (39) Miyata, M.; Nakajima, M.; Hashimoto, T. Impedance-matched dielectric metasurfaces for non-discrete wavefront engineering. *Journal of Applied Physics* **2019**, *125*, 103106.

Graphical TOC Entry

